Scientia Iranica B (2022) 29(5), 2317–2331

SCIENTIA IRANICA

Sharif University of Technology
Scientia Iranica
Transactions B: Mechanical Engineering
http://scientiairanica.sharif.edu

Entropy optimization of MHD Casson-Williamson fluid flow over a convectively heated stretchy sheet with Cattaneo-Christov dual flux

S. Eswaramoorthi[a] and S. Sivasankaran[b,*]

a. *Department of Mathematics, Dr. N.G.P. Arts and Science College, Coimbatore, Tamil Nadu, India.*
b. *Department of Mathematics, King Abdulaziz University, Jeddah 21589, Saudi Arabia.*

Received 9 May 2021; received in revised form 18 January 2022; accepted 13 June 2022

KEYWORDS
Casson-Williamson fluid;
Cattaneo-Christov double flux;
Homotopy analysis method;
Heat absorption.

Abstract. This work performs a comparative investigation into Casson-Williamson fluid flow over a heated porous stretchy sheet. The energy and mass transfer equations are modeled by Cattaneo-Christov theory. The governing flow models are altered into an Ordinary Differential Equation (ODE) model through proper transformations. The Homotopy Analysis Method (HAM) scheme is applied to determine the series solutions. The responses of diverse flow variables to fluid speed, fluid warmness, liquid concentration, skin friction coefficient, local Nusselt number, local Sherwood number, local entropy generation number, and Bejan number are analyzed through graphs and charts. It was found that the fluid speed would subside following an increase in values of the magnetic field, porosity, Casson fluid, Williamson fluid, and injection/suction parameters. The fluid warmness is increased due to high-level radiation, convective heating, and heat generation/absorption parameters and it suppresses the previous highs when enriching the convective cooling parameter. The chemical reaction parameter causes an increase in the thickness of the solutal boundary layer. The larger skin friction coefficient occurs in Casson fluid than Williamson fluid. The local entropy generation is attenuated upon increase in the Casson and Williamson parameters and it aggravates when the Biot number rises. The Bejan number is elevated when the Reynolds, Brinkman, and Biot numbers experience an increase.

1. Introduction

Most liquids in the industry are non-Newtonian and do not comply with Newton's law of motion. These fluids do not reside in a single constitutive rapport between the rate of deformation/strain and shear stresses. More researchers are expressing interest in developing non-Newtonian fluid flows with different physical configurations in recent decades by virtue of their industrial applications, such as wire drawing, glass blowing, hot rolling, foodstuffs, separation processes, etc. Casson fluid is one of the non-Newtonian fluid types that exhibits yield stress. The Casson fluid is of shear-thinning type and the rate of shear stress is infinite when viscosity is zero. When the shear stress is lower than the yield stress, this fluid behaves like a solid. When the shear stress is stronger than the yield stress applied, it behaves like a liquid and begins to move. Such fluids include honey, paints, tomato sauce, and intense fruit juices, to name a few. Nadeem et al. [1,2] scrutinized the predominance of Casson fluid flow on a stretching

*. *Corresponding author*
E-mail address: sd.siva@yahoo.com (S. Sivasankaran)

doi: 10.24200/sci.2022.58291.5654

sheet. Their results indicate that the thickness of a momentum boundary layer declines upon enhancing the value of the Casson fluid parameter. Shehzad et al. [3] examined the Magnetohydrodynamics (MHD) flow of a Casson fluid with suction and they proved that the fluid speed increased at higher Casson parameter value. The Casson fluid flow over an unsteady stretching sheet was revealed by Mukhopadhyay et al. [4] who identified that the fluid warmness was increased in the presence of the Casson parameter. The MHD flow of Casson nanofluid over a porous cylinder with Newtonian mass and heat conditions was presented by Naqvi et al. [5]. They proved that the fluid temperature was enhanced as the Casson parameter increased in value. Refs. [6–9] explored this area, which are worthy of consideration.

Another non-Newtonian type fluid is Williamson fluid that features shear thinning property. The study of Williamson fluid flows is more important because of its many applications in different areas of science and technology. The dual solutions of MHD Williamson fluid on a stretching sheet were derived by Hamid et al. [10]. They found that the velocity of the fluid decreases with Weissenberg number. Hashim et al. [11] revealed the significance of the 2D flow of time-dependent Williamson nanofluid on a moving wedge. They determined that the fluid temperature increased with respect to the presence of the Weissenberg number. The radiative 2D MHD flow of Williamson liquid on a time-dependent starching sheet was elucidated by Shah et al. [12]. Their outcome illustrates that the Weissenberg number leads to strengthening the sheet shear stress. Khan et al. [13] addressed the effect of temperature-dependent viscosity on Williamson nanofluid in nonlinear stretching sheet with thermal stratification. Zaman and Gul [14] reported the MHD fluid flow of a Williamson nanofluid with gyrotactic microorganisms. They found that the thickness of the momentum boundary layer declined when the Weissenberg number increased. Shashikumar et al. [15] investigated the time-independent MHD flow of Williamson fluid in a micro channel in the presence of Joule and viscous dissipation. Al-Sankoor et al. [16] examined the impact of Williamson nanofluid with magnetic effect. They noted that the fluid speed became slower when the Weissenberg number increased. Few crucial studies on this concept are found in [17–20].

The process of suction/injection plays an indispensable role in many industrial activities, like thermal oil recovery, radial diffusers, and thrust bearing design due to notable changes in the fluid flow field. Suction is used to eliminate unwanted reactants, whereas injection is applied to append reactants and reduce drag forces. In this view, Upreti et al. [21] derived the numerical solution of MHD flow of Ag-H_2O nanofluid on a flat plate with injection/suction. Their outcomes illustrate that the fluid velocity becomes small at larger values of injection/suction parameter. The impact of injection/suction of a Jeffery fluid past a stretching sheet with the influence of magnetic dipole was presented by Zeeshan and Majeed [22]. They proved that the fluid temperature decreased upon increase in the injection/suction values. Ramesh Babu et al. [23] addressed the Peristaltic transport of viscous fluid in a channel with suction/injection. The predominance of viscous dissipation and suction/injection of a second-grade fluid upon a stretching surface was disclosed by Bhuvaneswari et al. [24]. They found that the thickness of the velocity boundary layer was controlled by suction and improved by injection parameters. The impact of injection/suction of a micropolar hybrid nanofluid on a vertical plate was addressed by Gumber et al. [25]. They revealed that the fluid speed declined as injection/suction parameters decreased in value. Some sundry analyses on this area can be seen in [26–31].

Physically, entropy generation is used to measure the level of thermodynamic irreversibility in all types of heat transfer designs. The minimization of entropy generation technique is used to enhance thermal engineering devices for their superior efficiency. Different sources including a magnetic field, porous medium, fluid friction, viscous dissipation, and heat and mass transfer are responsible for the generation of entropy. Initially, entropy generation analysis was carried out by Bejan [32,33]. The 3D flow of a viscous fluid on an exponential stretching sheet with entropy generation was investigated by Afridi and Qasim [34]. They concluded that the Bejan number represented a non-increasing function of the Eckert number. Alzahrani et al. [35] deliberated on the consequences of thermal radiation on Casson fluid flow in a rectangular box. They observed that the Casson fluid would lead to the enrichment of the Bejan number. Yildiz et al. [36] examined the entropy generation of convective flow of air in a dome-shaped enclosure. The entropy generation Ag-H_2O nanofluid in a finned horizontal annulus was analyzed by Shahsavar et al. [37]. They proved that the frictional entropy generation was low at smaller Rayleigh numbers.

Therefore, motivated by the above-discussed works, our computational investigation focuses on the entropy optimization of MHD Casson-Williamson fluid flow along with a convectively heated stretchy sheet with Cattaneo-Christov dual theory. Many authors have examined the entropy analysis based on usual parameters including temperature difference parameter, Brinkman number, and local Reynolds number rather than the analysis featuring Casson parameter, Williamson parameter, suction/injection parameter, heat generation/absorption parameter, and Biot number. Thus, our current investigation is to fulfill this gap. The valuable outcomes of our study are the entryway for many scientists to initiate new

Table 1. Nomenclature

a	Constant
$Br\left(=\frac{\mu a^2 {x^*}^2}{k_0(T_f^*-T_\infty^*)}=\frac{kgm^{-1}s^{-1}m^2s^{-2}}{kgms^{-3}K^{-1}K}=1\right)$	Brinkman number
$Cr\left(=\frac{k_1^*}{a}=\frac{s^{-1}}{s^{-1}}=1\right)$	Chemical reaction parameter
De	Brownian diffusion coefficient
$fw\left(=-\frac{V_w^*}{\sqrt{a\nu}}=\frac{ms^{-1}}{\sqrt{s^{-1}m^2s^{-1}}}=1\right)$	Suction or injection parameter
$Ha\left(=\frac{\sigma B_0^2}{\rho a}=\frac{kg^{-1}m^{-2}s^3A^2m^{-1}kg^2s^{-4}A^{-2}}{s^{-1}kgm^{-3}}=1\right)$	Hartmann number
$Hg\left(=\frac{Q^*}{\rho a C_p}=\frac{kgm^2s^{-3}m^{-3}K^{-1}}{kgm^{-1}s^{-2}K^{-1}s^{-1}}=1\right)$	Heat generation or absorption parameter
h_w	Heat transfer coefficiet
k	Thermal conductive
k_1	Chemical reaction parameter
k^*	Mean absorption coefficient
$Pr\left(=\frac{\nu}{\alpha}=\frac{m^2s^{-1}}{m^2s^{-1}}=1\right)$	Prandtl number
Q	Heat generation/absorption coefficient
$Re\left(=\frac{a{x^*}^2}{\nu}=\frac{s^{-1}m^2}{m^2s^{-1}}=1\right)$	Local Reynolds number
$Rd\left(=\frac{4\sigma {T_\infty^*}^3}{kk^*}=\frac{4kgs^{-3}K^{-4}K^3}{kgms^{-3}K^{-1}m^{-1}}=constant\right)$	Radiation parameter
$Sc\left(=\frac{\nu}{De}=\frac{m^2s^{-1}}{m^2s^{-1}}=1\right)$	Schmidth number
T_f^*	The hot fluid temperature (K)
$u^*\&v^*$	Velocity components (ms^{-1})
V_w^*	Suction or injection parameter
$We\left(=\gamma x^*\sqrt{\frac{2a^3}{\nu}}=sm\sqrt{\frac{2s^{-3}}{m^2s^{-1}}}=constant\right)$	Williamson parameter
$x^*\&y^*$	Direction coordinates (m)
Greek symbols:	
α	Thermal diffusivity ($\mathrm{m^2s^{-1}}$)
β	Casson fluid parameter
$\gamma>0$	Time constant
$\Gamma\left(=\frac{\nu}{k_0 a}=\frac{m^2s^{-1}}{m^2s^{-1}}=1\right)$	Porosity parameter
$\Lambda_C\left(=\lambda_{C^*}a=ss^{-1}=1\right)$	Solutal relaxation time parameter
$\Lambda_T\left(=\lambda_{T^*}a=ss^{-1}=1\right)$	Thermal relaxation time parameter
ν	Kinematic viscosity ($\mathrm{m^2s^{-1}}$)
$\Omega\left(=\frac{T_f^*-T_\infty^*}{T_\infty^*}=\frac{K}{K}=1\right)$	Temperature difference parameter
ρ_f	Fluid density ($\mathrm{kgm^{-3}}$)
σ	Electrical conductivity
σ^*	Stefan Boltzmann constant ($\mathrm{Wm^{-2}K^{-4}}$)
Abbreviations:	
CF	Casson Fluid
CP	Concentration Profile
LNN	Local Nusselt Number
LSN	Local Sherwood Number
SFC	Ski Friction Coefficient
TP	Temperature Profile
WF	Williamson Fluid

thermal models in the industry. For the sake of affirmation, our attained results are comparatively found in agreement with those of formerly published works. All the emblematic estimations are carried out using Mathematica. The nomenclature is given in Table 1.

2. Mathematical formulation

This study consider the 2D steady, incompressible Casson-Williamson fluid flow along a stretchy paper with Cattaneo-Christov dual theory. The correlated velocities (u^*, v^*) are fixed with the Cartesian coordinates

(x^*, y^*). The static magnitude of the magnetic field B_0 is enforced in the y^*-direction and the created induced magnetic field was expunged due to the small Reynolds number. The velocity of the mass flux is denoted by V_w^* along with suction ($V_w^* < 0$) and injection ($V_w^* > 0$). The fluid temperature and concentration are disclosed by T_w^* and C_w^* and are considerably higher than the ambient temperature and concentration T_∞^* and C_∞^*, respectively. Novel characteristics of total entropy were computed through reversibility of heat and mass transfer and fluid friction. Heat generation/consumption and thermal radiation are added in energy transfer equations. Mass transfer attributes are scrutinized via a chemical reaction. The lower part of the sheet is warmed by hot fluid with warmness T_f^*, which creates a heat transfer coefficient h_w. The mathematical model, after employing the above assumptions, is presented as follows (see [38–41]):

$$u^*_{x^*} + v^*_{y^*} = 0, \tag{1}$$

$$u^* u^*_{x^*} + v^* v^*_{y^*} = \nu \left[1 + \frac{1}{\beta}\right] u^*_{y^*y^*} + \sqrt{2}\gamma u^*_{y^*} u^*_{y^*y^*} - \frac{\sigma B_0^2}{\rho} u^* - \frac{\nu}{k_0^*} u^*, \tag{2}$$

$$u^* T^*_{x^*} + v^* T^*_{y^*} = \alpha \left[1 + \frac{16\sigma^* {T_\infty^*}^3}{3kk^*}\right] T^*_{y^*y^*} - \Lambda_{T^*} \Big[u^* T^*_{x^*} u^*_{x^*} + v^* T^*_{y^*} v^*_{y^*} + {u^*}^2 T^*_{x^*x^*} + {v^*}^2 T^*_{y^*y^*} + 2u^* v^* T^*_{x^*y^*} + u^* T^*_{y^*} v^*_{x^*} + v^* T^*_{x^*} u^*_{y^*}\Big] + \frac{Q^*}{\rho C_p}(T^* - T^*_\infty), \tag{3}$$

$$u^* C^*_{x^*} + v^* C^*_{y^*} = De C^*_{y^*y^*} - \Lambda_{C^*} \Big[u^* C^*_{x^*} u^*_{x^*} + v^* C^*_{y^*} v^*_{y^*} + {u^*}^2 C^*_{x^*x^*} + {v^*}^2 C^*_{y^*y^*} + 2u^* v^* C^*_{x^*y^*} + u^* C^*_{y^*} v^*_{x^*} + v^* C^*_{x^*} u^*_{y^*}\Big] - k_1^*(C^* - C^*_\infty). \tag{4}$$

Boundary conditions:

$$u^* = U_w^*(x^*), \quad v^* = V_w^*, \quad -kT^*_{y^*} = h_w(T_f^* - T^*), \quad C^* = C_w^* \quad \text{at} \quad \eta \to 0,$$

$$u^* \to 0, \quad u^*_{y^*} \to 0, \quad T^* \to T^*_\infty, \quad C^* \to C^*_\infty, \quad \text{as} \quad \eta \to \infty, \tag{5}$$

where (u^*,v^*) are the velocity factors in (x^*,y^*) directions, ν is the kinematic viscosity, β the Casson fluid parameter, $\gamma > 0$ the time constant, σ electrical conductivity, ρ density, Cp specific heat, k_0^* the porosity, α the thermal diffusivity, σ^* the Stefan-Boltzmann constant, k^* the mean absorption coefficient, k thermal conductivity, Λ_{T^*} the thermal relaxation time of the heat diffusion, Λ_{C^*} the concentration relaxation time of the mass diffusion, Q^* heat source/sink parameter, De the Brownian diffusion coefficient, k_1^* the first order chemical reaction parameter, h_w the heat transfer coefficient, T_f^* the hot fluid temperature, and V_w^* the suction or injection parameter. Define:

$$\eta = y^* \sqrt{\frac{b}{\nu}}, \quad u^* = ax^* f', \quad v^* = -\sqrt{a\nu} f,$$

$$\theta = \frac{T^* - T^*_\infty}{T_f^* - T^*_\infty}, \quad \phi = \frac{C^* - C^*_\infty}{C^*_w - C^*_\infty}. \tag{6}$$

Implementing Eq. (6) on Eqs. (2)–(4), we get:

$$\left[1 + \frac{1}{\beta}\right] f''' - f'^2 + ff'' + Wef''f''' - [Ha + \Gamma] f' = 0, \tag{7}$$

$$\frac{1}{Pr}\left[1 + \frac{4}{3}Rd\right]\theta'' + f\theta' - \Lambda_T \left[ff'\theta' + f^2\theta''\right] + Hg\theta = 0, \tag{8}$$

$$\frac{1}{Sc}\phi'' + f\phi' - \Lambda_C\left[ff'\phi' + f^2\phi''\right] - Cr\phi = 0. \tag{9}$$

With the associated conditions:

$$f(0) = fw, \quad f'(0) = 1, \quad \theta'(0) = -Bi\left[1 - \theta(0)\right],$$

$$\phi(0) = 1, \quad f'(\infty) = 0, \quad f''(\infty) = 0, \quad \theta(\infty) = 0,$$

$$\phi(\infty) = 0, \tag{10}$$

where $We = \gamma x^* \sqrt{\frac{2a^3}{\nu}}$ is the Williamson parameter, $Ha = \frac{\sigma B_0^2}{\rho a}$ the Hartmann number, $\Gamma = \frac{\nu}{k_0 a}$ the porosity parameter, $Pr = \frac{\nu}{\alpha}$ the Prandtl number, $Rd = \frac{4\sigma {T_\infty^*}^3}{kk^*}$ the radiation parameter, $\Lambda_T = \lambda_{T^*} a$ the thermal relaxation time parameter, $Hg = \frac{Q^*}{\rho a C_p}$ the heat generation or absorption parameter, $Sc = \frac{\nu}{De}$ the Schmidth number, $\Lambda_C = \lambda_{C^*} a$ the solutal relaxation time parameter, $Cr = \frac{k_1^*}{a}$ the chemical reaction parameter, $fw = -\frac{V_w^*}{a\nu}$ the suction or injection parameter, and $Bi = \frac{h_w}{k}\sqrt{\frac{\nu}{a}}$ the Biot number.

The Skin Friction Coefficient (SFC), Local Nusselt Number (LNN), and Local Sherwood Number (LSN) are written as follows:

$$c_f = \frac{\tau_w^*}{\rho U_w^{*2}/2}, \quad Nu = \frac{x^*(q_w^* + q_r^*)}{k(T_w^* - T_\infty^*)}, \quad \text{and}$$

$$Sh = \frac{x^* j_w^*}{D_B^*(C_w^* - C_\infty^*)},$$

where:

$$\tau_w^* = \left[\mu + \frac{p_{y^*}}{\sqrt{2\pi}}\right]\left(\frac{\partial u^*}{\partial y^*}\right)_{y^*=0},$$

is the wall shear stress for Casson fluid,

$$\tau_w^* = \mu\left(\frac{\partial u^*}{\partial y^*} + \frac{\Gamma}{\sqrt{2}}\left[\frac{\partial u^*}{\partial y^*}\right]^2\right)_{y^*=0},$$

is the wall shear stress for Williamson fluid,

$$q_w^* = -\left(k\frac{\partial T^*}{\partial y^*} + \frac{4\sigma^*}{3k^*}\frac{\partial T^{*^4}}{\partial y^*}\right)_{y^*=0},$$

is the surface heat flux and

$$j_w^* = -k\left(\frac{\partial C^*}{\partial y^*}\right)_{y^*=0},$$

is the surface mass flux.

The reduced form of SFC, LNN, and LSN are expressed as follows:

$$\frac{1}{2}Cf\sqrt{Re} = \left(1 + \frac{1}{\beta}\right)f''(0)$$

for Casson fluid;

$$\frac{1}{2}Cf\sqrt{Re} = \left(f''(0) + \frac{We}{2}f''(0)\right)f''(0)$$

for Williamson fluid;

$$Nu/\sqrt{Re} = -\left(1 + \frac{4}{3}R\right)\theta'(0), \quad \text{and}$$

$$Sh/\sqrt{Re} = -\phi'(0).$$

3. Entropy analysis

The dimensional form of the entropy generation is expressed below (see [42,43]):

$$S_{gen} = \frac{k}{T^{*3}_\infty}\left[1 + \frac{16\sigma T_\infty^{*^3}}{3kk^*}\right]T_{y^*}^{*^2} + \frac{\mu}{T_\infty^*}\left\{\left[1 + \frac{1}{\beta}\right]u_{y^*}^{*^2} + \sqrt{2}\Gamma u_{y^*}^{*^3}\right\} + \frac{\sigma B_0^2}{T_\infty^*}u^{*^2} + \frac{\mu}{T_\infty^* k_0^*}u^{*^2}. \tag{11}$$

After applying suitable transformations, we get:

$$EG = Re\left[1 + \frac{4}{3}Rd\right]\theta'^2 + ReBr\frac{1}{\Omega}\left[\left(1 + \frac{1}{\beta}\right)f''^2 + \frac{We}{\sqrt{2}}f'''^3\right] + ReBr\frac{1}{\Omega}[Ha + \Gamma]f'^2, \tag{12}$$

where $Re = \frac{ax^{*^2}}{\nu}$ is the local Reynolds number, $Br = \frac{\mu a^2 x^{*^2}}{k(T_f^* - T_\infty^*)}$ the Brinkman number and $\Omega = \frac{T_f^* - T_\infty^*}{T_\infty^*}$ the temperature difference parameter. The Bejan number is defined as follows:

$$BE = \frac{\text{Entropy generation due to heat and mass transfer}}{\text{Total entropy generation}}, \tag{13}$$

$$BE = \frac{N_1}{N_2}, \tag{14}$$

$$N_1 = Re\left[1 + \frac{4}{3}Rd\right]\theta'^2, \tag{15}$$

$$N_2 = Re\left[1 + \frac{4}{3}Rd\right]\theta'^2 + ReBr\frac{1}{\Omega}\left[\left(1 + \frac{1}{\beta}\right)f''^2 + \frac{We}{\sqrt{2}}f'''^3\right] + ReBr\frac{1}{\Omega}[Ha + \Gamma]f'^2. \tag{16}$$

4. HAM solution

The reduced ODE's (7)–(9) and their associated conditions (10) are solved using Homotopy Analysis method (HAM) procedure, see Eswaramoorthi et al. [44]. In this respect, the initial rule is selected as $f_0(\eta) = fw + 1 - \frac{1}{e^\eta}$, $\theta_0(\eta) = \frac{Bi}{(1+Bi)e^\eta}$ and $\phi_0(\eta) = \frac{1}{e^\eta}$. The corresponding linear operators are $L_f = D^3 f - Df$, $L_\theta = D^2\theta - \theta$ and $L_\phi = D^2\phi - \phi$, here $D = \frac{d}{d\eta}$ with the property $L_f\left[A_1 + A_2 e^\eta + \frac{A_3}{e^\eta}\right] = L_\Theta\left[A_4 e^\eta + \frac{A_5}{e^\eta}\right] = L_\phi\left[A_6 e^\eta + \frac{A_7}{e^\eta}\right] = 0$ where $A_j (j = 1-7)$ are constants.

After substituting the ith-order HAM equations, we get:

$$f_i(\eta) = f_i^*(\eta) + A_1 + A_2 e^\eta + \frac{A_3}{e^\eta},$$

$$\theta_i(\eta) = \theta_i^*(\eta) + A_4 e^\eta + \frac{A_5}{e^\eta},$$

$$\phi_i(\eta) = \phi_i^*(\eta) + A_6 e^\eta + \frac{A_7}{e^\eta}.$$

Herein, the particular solutions are $f_i^*(\eta)$, $\theta_i^*(\eta)$ and $\phi_i^*(\eta)$.

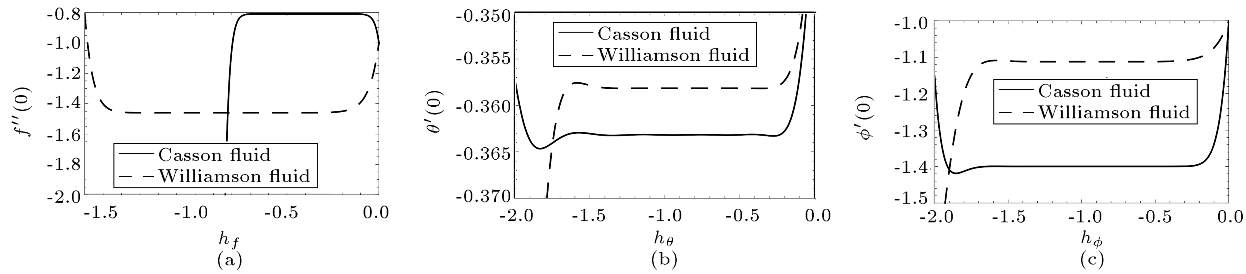

Figure 1. The h curves of velocity: (a) Temperature, (b) concentration, and (c) profiles for both fluids.

Table 2. Comparison of SKC with Shehzad et al. [38]

β	M	fw	$-\frac{1}{2}Cf\sqrt{Re}$ Present study	$-\frac{1}{2}Cf\sqrt{Re}$ Shehzad et al. [38]
0.5	0.5	0.5	2.20256	2.20256
0.8			1.94558	1.94558
1.3			1.75799	1.75799
2.0			1.64194	1.64195
0.8	0.0	0.5	1.77069	1.77069
	0.6		2.01706	2.01706
	1.2		2.60637	2.60638
	1.5		2.96570	2.96570
0.8	0.5	0.0	1.67705	1.67705
		0.7	2.06318	2.06318
		1.4	2.51728	2.51728
		2.0	2.95256	2.95256

Table 3. Comparison of $-f''(0)$ with different values of We with Nadeem and Hussain [39] and Nadeem and Hussain [20].

Order	$We = 0.1$ Present study	$We = 0.1$ Nadeem and Hussain [39]	$We = 0.2$ Present study	$We = 0.2$ Nadeem and Hussain [20]
1	1.03000	1.04	1.06	1.047
5	1.03448	1.03446	1.07619	1.076
10	1.03446	1.03446	1.07621	1.076
15	1.03446	1.03446	1.07621	1.076

Table 4. Order of approximations.

Order	Cassson fluid $-f''(0)$	Cassson fluid $-\theta'(0)$	Cassson fluid $-\phi'(0)$	Williamson fluid $-f''(0)$	Williamson fluid $-\theta'(0)$	Williamson fluid $-\phi'(0)$
1	0.82667	0.32146	1.29310	1.39000	0.32146	1.36810
5	0.80845	0.32845	1.39970	1.45780	0.32160	1.51956
10	0.80836	0.32817	1.39965	1.45981	0.32163	1.52035
15	0.80836	0.32817	1.39959	1.45982	0.32163	1.52035
20	0.80836	0.32817	1.39959	1.45982	0.32163	1.52035
25	0.80836	0.32817	1.39959	1.45982	0.32163	1.52035
30	0.80836	0.32817	1.39959	1.45982	0.32163	1.52035
35	0.80836	0.32817	1.39959	1.45982	0.32163	1.52035
40	0.80836	0.32817	1.39959	1.45982	0.32163	1.52035

These series solutions include the parameters (h_f, h_θ, h_ϕ) and they handle the solution convergency. From Figure 1(a)–(c), the range values of h_f, h_θ, and h_ϕ in Casson fluid are $-0.7 \leq h_f \leq -0.1$, $-1.3 \leq h_\theta \leq -0.4$, $-1.5 \leq h_\phi \leq -0.4$ and those in Williamson fluid are $-1.4 \leq h_f \leq -0.3$, $-1.4 \leq h_\theta \leq -0.4$ and $-1.6 \leq h_\phi \leq -0.3$. For more accuracy of our results, we fix $h_f = -0.4$ and $h_\theta = h_\phi = -0.9$ for Casson fluid and $h_f = h_\theta = h_\phi = -0.9$ for Williamson fluid.

5. Results and discussion

This section presents the numerical and graphical results of fluid velocity, fluid temperature, fluid concentration, SFC, LNN, LSN, entropy generation, and Bejan number for diverse flow parameters with a constant quantity of Prandtl number (Pr = 1.2) and Schmidt number (Sc = 1.0). Table 2 portrays the comparison of SKC with Shehzad et al. [38] for different values of β, M, and fw. Comparison of $-f''(0)$ with different values of We with Nadeem and Hussain [39] and Nadeem and Hussain [20] is illustrated in Table 3. From Tables 2 and 3, we see that our results are in good agreement. Table 4 shows the order of approximation of HAM method and it is seen that 15th order is sufficient for taking results. Table 5 provides the predominance of SFC, LNN, and LSN for various of β, We, Γ, M, and fw. We realize that the surface shear stress increases in the presence of β and We. On the other hand, it is reduced at surging values of Γ, M, and fw for both fluids. The LNN wanes due to the availability of β, We, Γ, and M. However, it enlarges

Table 5. Skin friction coefficient, local Nusselt number and local Sherwood number for different values of β, We, Γ, M and fw.

β/We	Γ	M	fw	Cassson			Williamson		
				$\frac{1}{2}Cf\sqrt{Re}$	$\frac{Nu}{\sqrt{Re}}$	$\frac{Sh}{\sqrt{Re}}$	$\frac{1}{2}Cf\sqrt{Re}$	$\frac{Nu}{\sqrt{Re}}$	$\frac{Sh}{\sqrt{Re}}$
0.5/0.0	0.2	0.3	0.3	−2.27662	0.54780	1.40357	−1.38390	0.53671	1.36088
1.0/0.1				−1.88853	0.54422	1.38925	−1.35326	0.53605	1.35808
1.5/0.2				−1.73824	0.54236	1.38224	−1.31874	0.53527	1.35479
2.0/0.3				−1.65748	0.54124	1.37803	−1.27751	0.53433	1.35071
2.5/0.4				−1.60688	0.54050	1.37522	−1.20699	0.53308	1.34515
3.0/0.5				−1.57214	0.53997	1.37320	−0.80311	0.53111	1.33609
0.6/0.1	0.0	0.3	0.3	−2.01793	0.54804	1.40374	−1.27302	0.53738	1.36317
	0.3			−2.22103	0.54644	1.39767	−1.39130	0.53544	1.35575
	0.5			−2.34602	0.54549	1.39406	−1.46384	0.53431	1.35143
	0.8			−2.52118	0.54419	1.38917	−1.56535	0.53281	1.34568
	1.0			−2.63110	0.54341	1.38619	−1.63269	0.53194	1.34241
0.6/0.1	0.2	0.0	0.3	−1.94513	0.54864	1.40599	−1.23050	0.53811	1.36595
		0.3		−2.15562	0.54695	1.39960	−1.35326	0.53605	1.35808
		0.5		−2.28444	0.54596	1.39583	−1.42813	0.53486	1.35354
		0.8		−2.46427	0.54461	1.39074	−1.53231	0.53329	1.34750
		1.0		−2.57676	0.54373	1.38765	−1.59822	0.53236	1.34395
0.6/0.1	0.2	0.3	−1.0	−1.56155	0.41170	0.79921	−0.80423	0.40344	0.78640
			−0.5	−1.76556	0.46203	0.96139	−0.97697	0.45181	0.94045
			0.0	−2.00000	0.51450	1.19785	−1.19697	0.50344	1.16545
			0.5	−2.26556	0.56901	1.57358	−1.46752	0.55848	1.52470
			1.0	−2.56155	0.62691	2.26214	−1.78610	0.61725	2.18558

at higher values of fw on both fluids. The same trend was obtained in the LSN case.

Figure 2(a)–(f) delineate the streamline for CF and WF for $fw = 1.0$, 0.0 and -1.0. The prominence of M and Γ on the fluid velocity profile in the case of Casson and Williamson fluids is presented in Figure 3(a) and (b). It was found that the fluid speed was reduced as the values of M and Γ for both fluids increased. The magnetic field parameter generates a drag force called the Lorentz force which suppresses the fluid motion, thus slowing down the fluid speed. Figure 4(a) and (b) present the variations of velocity profile at different values of fw, β, and We. It is noticed that the fluid speed subsides due to the stronger presence of fw, β, and We. Physically, larger magnitude of β, enhances the plastic dynamic viscosity which forms a resistive

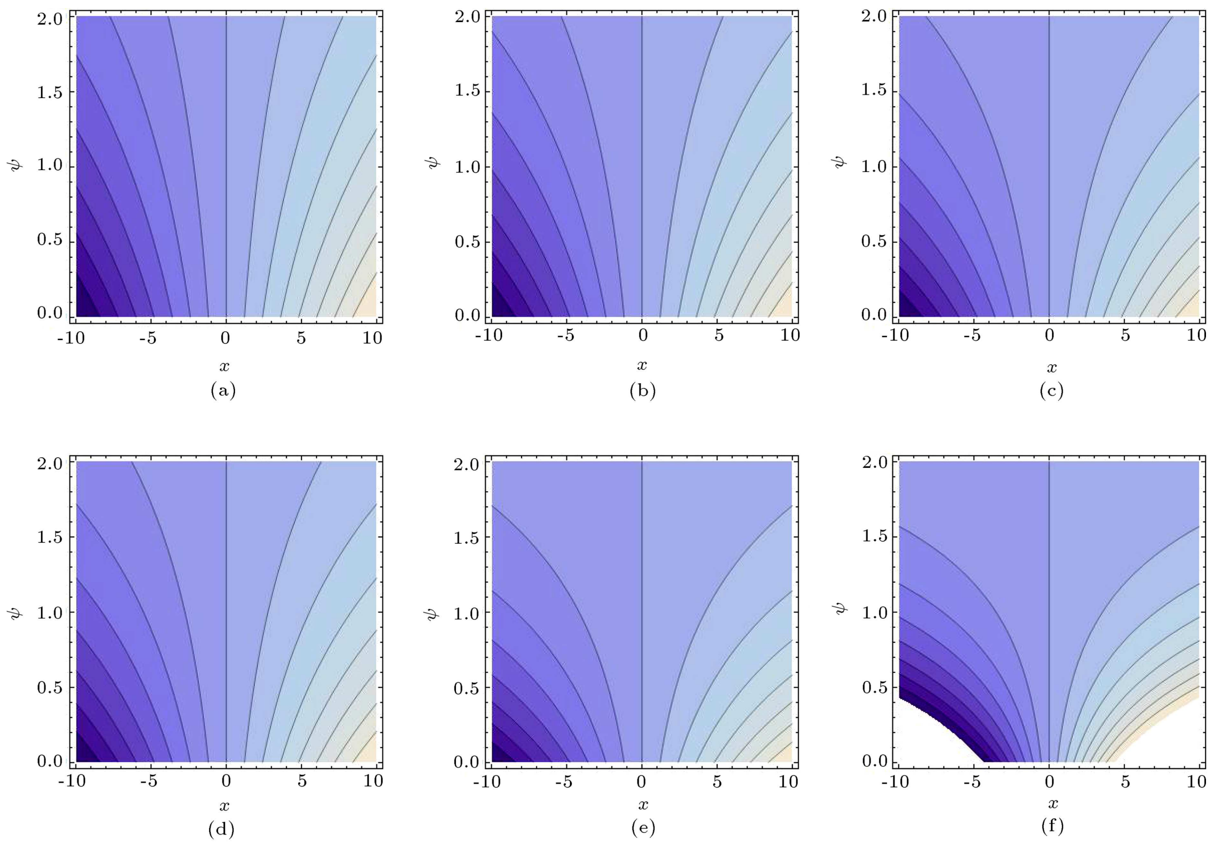

Figure 2. Stream line on Casson fluid (a)–(c) and Williamson fluid (d)–(f) for $fw = 1.0$ (a, d), $fw = 0.0$ (b, e) and $fw = -1.0$ (c, f).

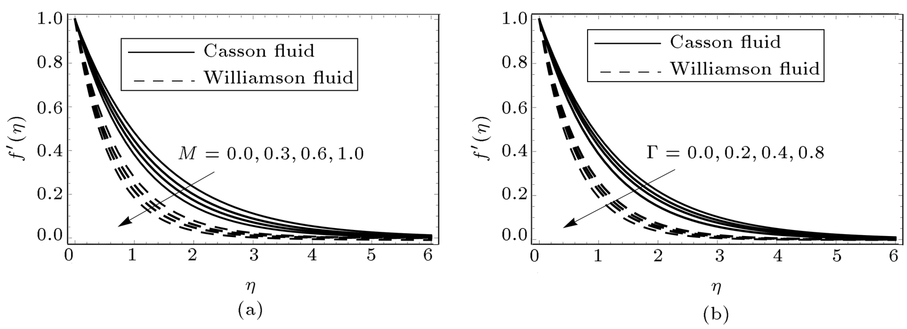

Figure 3. Velocity profile at different values of (a) M and (b) Γ for both fluids.

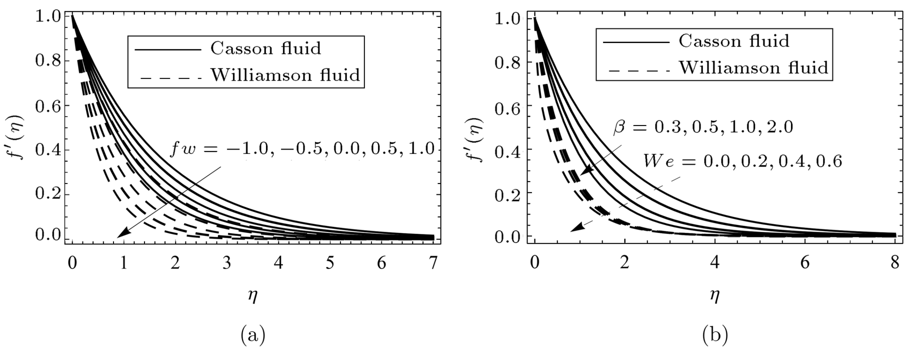

Figure 4. Velocity profile at different values of (a) fw and (b) β variations for Casson fluid and We variations for Williamson fluid.

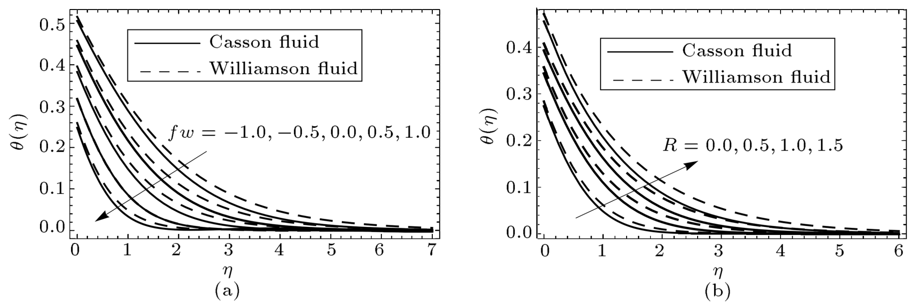

Figure 5. Temperature profile at different values of (a) fw and (b) R for both fluids.

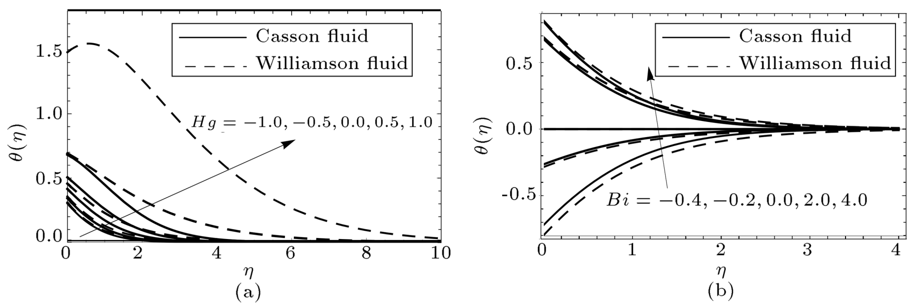

Figure 6. Temperature profile at different values of (a) Hg and (b) Bi for both fluids.

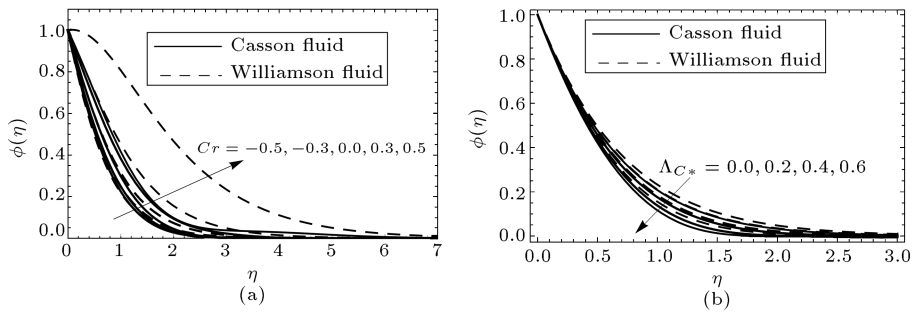

Figure 7. Concentration profile at different values of (a) Cr and (b) Λ_{C*} for both fluids.

force in the flow, leading to slowdown of the fluid speed. The impact of fw and R on temperature profile on temperature profile in both of the fluids is described in Figure 5(a) and (b). It is identified that the fluid warmness increases upon enriching R values and it decreases upon increasing fw values. Figure 6(a) and (b) portray the changes in TP at different values of Hg and Bi for both fluids. It is seen that the fluid gets warm due to the presence of Hg and Bi for both fluids. Physically, the ascending values of Hg elevate the fluid thermal state and this leads to increased fluid temperature, although the large Biot number forms a greater heat transfer coefficient, thus enriching the fluid temperature. The impact of Cr and Λ_C on CP was illustrated in Figure 7(a) and (b). It is found that the fluid enhances the concentration at a greater value of Cr and reduces the concentration at higher Λ_C values.

Figure 8(a) and (b) render the SFC for ascending values of M, fw, and Γ for both fluids. Here it is noticed that the surface shear stress is reduced when the values of M, fw, and Γ increase. The LNN for different combination of M, fw, and Γ is plotted in Figure 9(a) and (b). According to these figures, the HT gradient slightly increases upon enhancing the values of fw and remains almost the same as the values of M and Γ increase. Figure 10(a) and (c) exhibit the impact of Λ_T, Hg, R, and Bi on LNN for both fluids. It was realized that the HT gradients would experience a decrease given Hg in Williamson fluid and opposite behavior obtained in Casson fluid. Moreover, the HT gradient remained almost the same when Λ_T changes. In the case of Williamson fluid, the LNN escalates in the heat absorption case, while it dwindles in the heat generation case for enhancing the value of radiation parameter. The rate of heat transfer variation increases with increase in the Bi values. On the contrary, the opposite trend was attained in Casson fluid in the presence of Rd and Bi. Figure 11(a) and (b) show

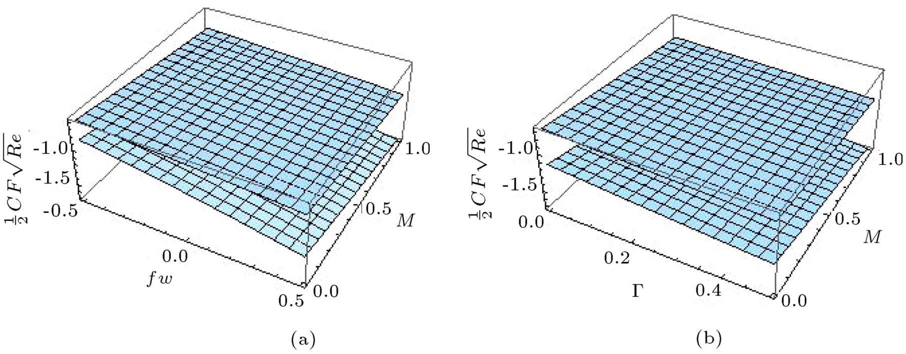

Figure 8. Skin friction coefficient at different combinations of M, fw, and Γ for Casson fluid (upper plate) and Williamson fluid (lower plate).

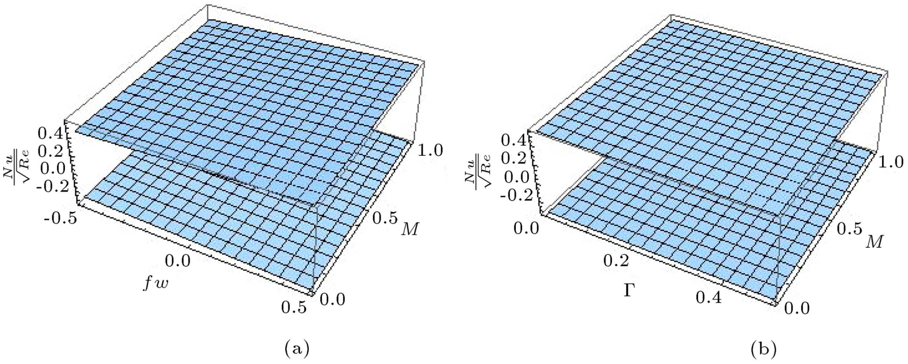

Figure 9. Local Nusselt number for different combinations of M, fw, and Γ for Casson fluid (lower plate) and Williamson fluid (upper plate).

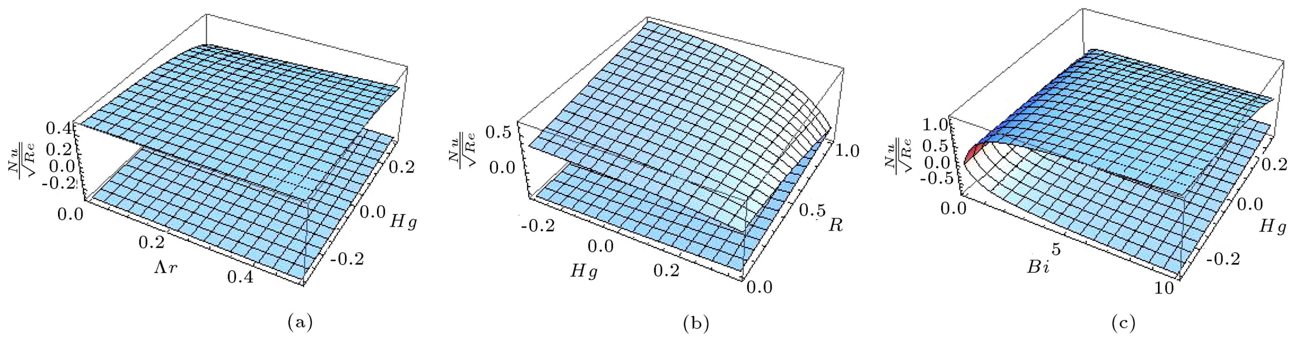

Figure 10. Local Nusselt number for different combinations of ΛT, Hg, R, and Bi for Casson fluid (lower plate) and Williamson fluid (upper plate).

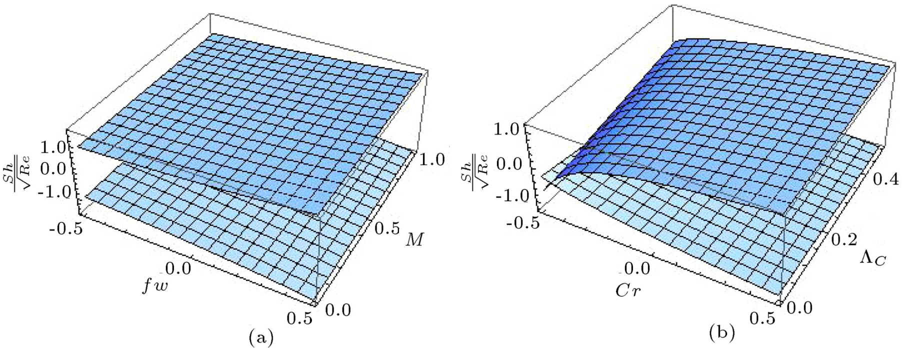

Figure 11. Local Sherwood number for different combination of M, fw, and Γ for Casson fluid (lower plate) and Williamson fluid (upper plate).

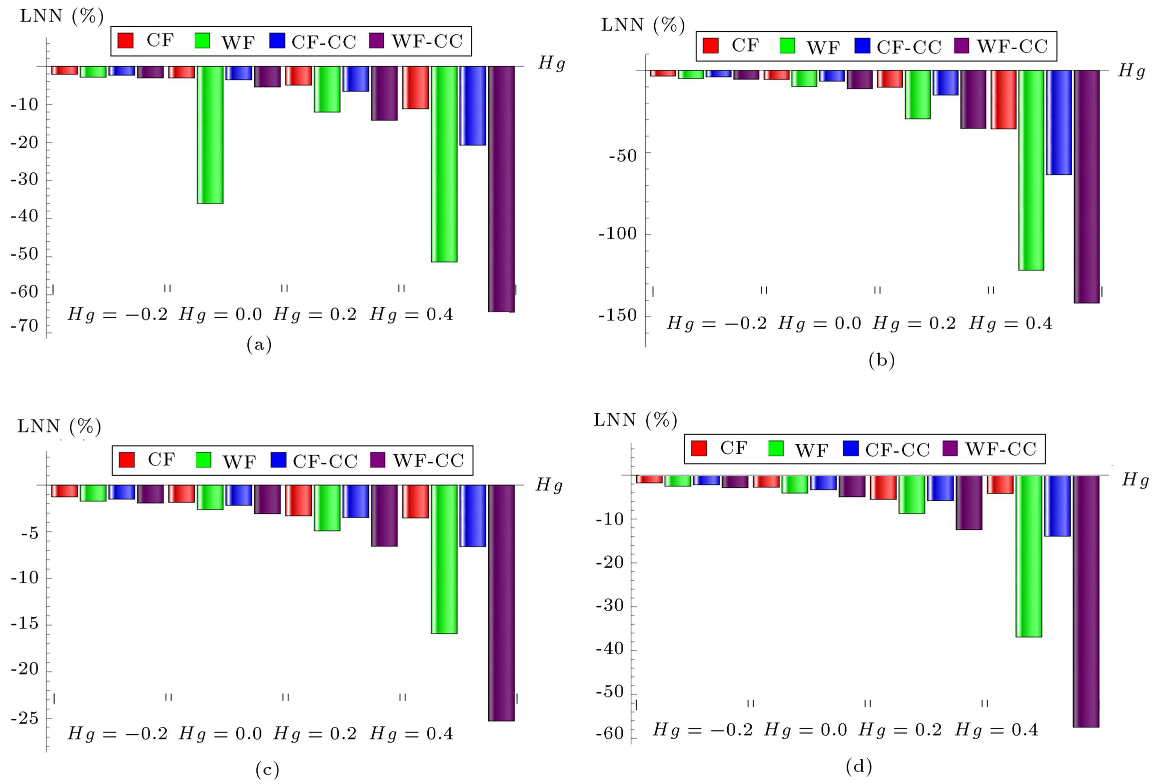

Figure 12. Decrement percentage of local Nusselt number at different values of Hg and Λ_T with (a) $R = 0.5$ & $Bi = 0.2$, (b) $R = 0.5$ & $Bi = -0.2$, (c) $R = 0.0$ & $Bi = 0.2$, and (d) $R = 0.0$ & $Bi = -0.2$.

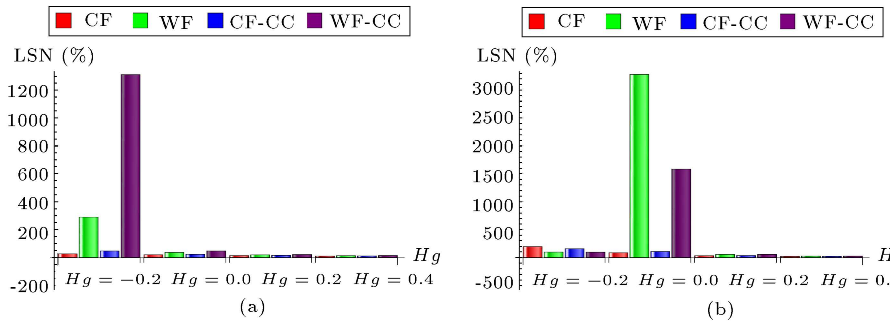

Figure 13. Increment percentage of local Sherwood number at different values of Cr and Λ_C with (a) $fw = 0.3$ and (b) $fw = -0.3$.

the LNN at different values of fw, M, Cr, and Λ_C for both fluids. It is noted that the mass transfer gradient remains almost the same at M and Λ_C values for both fluids. The LNN is upgraded upon increasing fw and Cr values in WF and it declines in CF.

Figure 12(a)–(d) portray the decrement percentage of LNN at different values of Hg various combination of R and Bi. It is proved that the decrement percentage is high when Hg varies from 0.2 to 0.4 in WF without CCDF, and minimum decrement percentage occurs in CF with CCDF in Hg which varies from -0.4 to -0.2. In all cases, the decrement percentage is lower in the CCDF model than that in Fourier model. In addition, the CF experiences a lower percentage of decrement than WF. The increment percentage of LSN for different combinations of Hg, fw, Cr, and Λ_C was illustrated in Figure 13(a) and (b). In suction flow, it is found that WF without CCDF has a higher increment percentage when Cr varies from -0.4 to -0.2, while a lower increment percentage occurs in CF with CCDF when Cr varies from 0.2 to 0.4. However, in the injection case, WF with CCDF has a higher increment percentage when Cr varies from -0.2 to 0.0, and smaller increment percentage is obtained in CF with CCDF when Cr varies from 0.2 to 0.4. In addition, the CF has a lower increment percentage than WF.

Entropy generation at different values of β, We, fw, Bi, and Hg is displayed in Figure 14(a)–(d). It is concluded from these figures that EG suppresses at

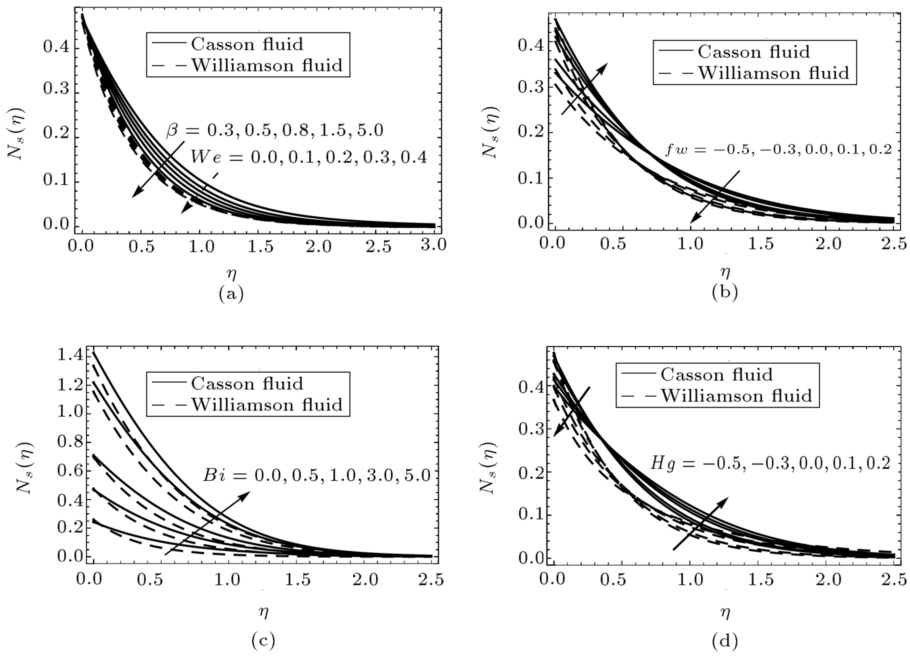

Figure 14. Entropy generation at different values of β, We, fw, Bi, and Hg.

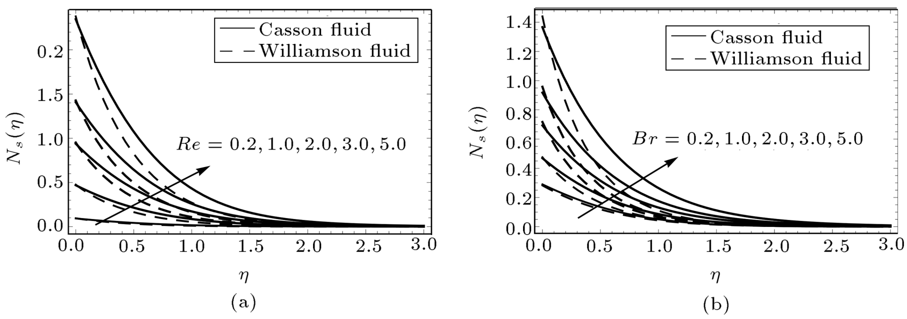

Figure 15. Entropy generation at different values of Re and Br.

high values of β and We and it is boosted up when Bi values increase. Besides, EG enhances near the plate and suppresses away from the surface at fw values. The opposite trend was observed at Hg values. A higher value of Bi enriches the heat transfer rate, which enhances the entropy generation. The higher quantity of Brinkman number facilitates suppressing the fluid thermal conductivity, thus enriching the entropy generation. Figure 15(a) and (b) explain the changes of EG with respect to Re and Br. It was found that EG increased when the values of Re and Br increased for both fluids. The Bejan number at different values of β, We, Hg, Bi, and Br were plotted in Figure 16(a)–(d). It is noted that the Bejan number increases at higher values of β, We, Br, Hg, and Bi and it declines at a higher value of Br.

6. Conclusions

The entropy optimization of a Williamson-Casson fluid over a stretching sheet with convective boundary condition was investigated. The energy and mass equations were framed based on Cattaneo-Christov heat-mass flux theory. The Homotopy Analysis Method (HAM) procedure was applied to solve the obtained Ordinary Differential Equations (ODEs). The salient features of our investigations are summarized below:

- The fluid velocity declined when the porosity and magnetic field parameters were strengthened;
- The fluid temperature increased when the radiation and heat generation/absorption parameters increased;
- The fluid concentration upsurged as the chemical reaction parameter increased;
- The heat transfer gradient was attenuated upon enhancing the radiation and heat generation/absorption parameters;
- The local entropy generation declined by increasing the Casson and Williamson parameters;

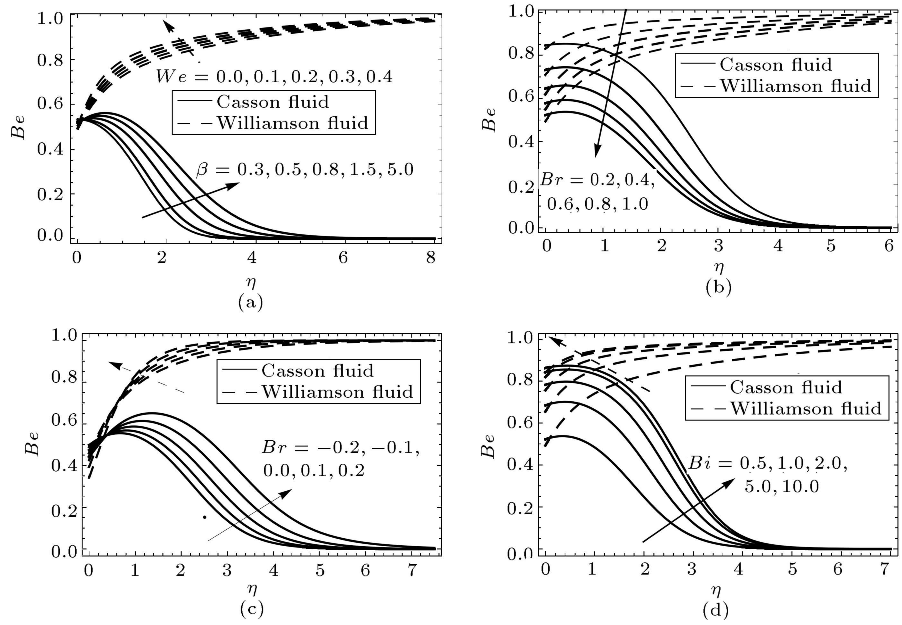

Figure 16. Bejan number at different values of β, Br, and Hg.

- The Bejan number was escalated when the Biot number and heat generation/absorption parameter increased in value.

References

1. Nadeem, S., Haq, R.U., Akbar, N.S., et al. "MHD three-dimensional Casson fluid flow past a porous linearly stretching sheet", *Alex. Eng. J.,* **52**, pp. 577–582 (2013).

2. Nadeem, S, Haq, R.U., and Lee, C. "MHD flow of a Casson fluid over an exponentially shrinking sheet", *Sci. Iran., B.,* **19**, pp. 1550–1553 (2012).

3. Shehzad, S.A., Hayat, T., Qasim, M., et al. "Effects of mass transfer on MHD flow of Casson fluid with chemical reaction and suction", *Braz. J. Chem. Eng.,* **30**(01), pp. 187–195 (2013).

4. Mukhopadhyay, S., Ranjan, D.P., Bhattacharyya, K., et al. "Casson fluid flow over an unsteady stretching surface", *Ain Shams Eng. J.,* **4**, pp. 933–938 (2013).

5. Naqvi, S.M.R.S., Muhammad, T., and Asma, M. "Hydromagnetic flow of Casson nanofluid over a porous stretching cylinder with Newtonian heat and mass conditions", *Phys. A: Stat. Mech. Appl.,,* **550**, p. 123988 (2020).

6. Pramanik, S. "Casson fluid flow and heat transfer past an exponentially porous stretching surface in presence of thermal radiation", *Ain Shams Eng. J.*, **5**, pp. 205–212 (2014).

7. Atif, S.M., Shah, S., and Kamran, A. "Effect of MHD on Casson fluid with Arrhenius activation energy and variable properties", *Scientia Iranica, F* (2022) (In Press). https://dx.doi.org/10.24200/sci.2021.57873.5452

8. Makinde, O.D. and Gnaneswara Reddy, M. "MHD peristaltic slip flow of Casson fluid and heat transfer in channel filled with a porous medium", *Scientia Iranica,,* **26(4)**, pp. 2342–2355 (2019).

9. Kameswarn, P.K., Shaw, S., and Sibanda, P. "Dual solutions of Casson fluid flow over a stretching or shrinking sheet", *Sadhana,* **39**, pp. 1573–1583 (2014).

10. Hamid, A., Hashim, Khan, M., and Hafeez, A. "Unsteady stagnation-point flow of Williamson fluid generated by stretching/shrinking sheet with Ohmic heating", *Int. J. Heat Mass Transf.,* **126**, pp. 933–940 (2018).

11. Hashim, Khan, M. and Hamid, A. "Numerical investigation on time-dependent flow of Williamson nanofluid along with heat and mass transfer characteristics past a wedge Geometry", *Int. J. Heat Mass Transf.,* **118**, pp. 480–491 (2018).

12. Shah, Z., Bonyah, E., Islam, S., et al. "Radiative MHD thin film flow of Williamson fluid over an unsteady permeable stretching sheet", *Heliyon,* **4**, e00825, pp. 1–20 (2018).

13. Khan, M., Salahuddin, T., Malik, M.Y., et al. "Change in viscosity of Williamson nanofluid flow due to thermal and solutal stratification", *Int. J. Heat Mass Transf.,* **126**, pp. 941–948 (2018).

14. Zaman, S. and Gul, M. "Magnetohydrodynamic bioconvective flow of Williamson nanofluid containing gyrotactic microorganisms subjected to thermal radiation and Newtonian conditions", *J. Theor. Biol.,* **479**, pp. 22–28 (2019).

15. Shashikumar, N.S., Madhu, M., Sindhu, S., et al. "Naikoti Kishan, Thermal analysis of MHD Williamson fluid flow through a microchannel", *Int. Commun. Heat Mass Transf.*, **127**, p. 105582 (2021).

16. Al-Sankoor, K., Al-Gayyim, H., Al-Musaedi, S., et al. "Analytically investigating of heat transfer parameters with presence of graphene oxide nanoparticles in Williamson-magnetic fluid by AGM and HPM methods", *Case Stud. Therm. Eng.*, **27**, p. 101236 (2021).

17. Bilal, M., Sagheer, M., and Hussain, S. "Numerical study of magnetohydrodynamics and thermal radiation on Williamson nanofuid flow over a stretching cylinder with variable thermal conductivity", *Alex Eng J.,* **57**, pp. 3281–3289 (2018).

18. Khan, N.A. and Khan, H. "A boundary layer flows of non-Newtonian Williamson fluid", *Nonlinear Eng.,* **3**, pp. 107–115 (2014).

19. Malik, M.Y. and Salahuddin, T. "Numerical solution of MHD stagnation point flow of Williamson fluid model over a stretching cylinder", *Int. J. Nonlin. Sci. Num.,* **16**, pp. 161–164 (2015).

20. Nadeem, S. and Hussain, S.T. "Flow and heat transfer analysis of Williamson nanofluid", *Appl. Nanosci.,* **4**, pp. 1005–1012 (2014).

21. Upreti, H., Pandey, A.K., and Kumar, M. "MHD flow of Ag-water nanofluid over a flat porous plate with viscous-Ohmic dissipation, suction/injection and heat generation/absorption", *Alex. Eng. J.,* **57(3)**, pp. 1839–1847 (2018).

22. Zeeshan, A. and Majeed, A. "Heat transfer analysis of Jeffery fluid flow over a stretching sheet with suction/injection and magnetic dipole effect", *Alex. Eng. J.,* **55**, pp. 2171–2181 (2016).

23. Ramesh Babu, V., Sreenadh, S., and Srinivas, A.N.S. "Peristaltic transport of a viscous fluid in a porous channel with suction and injection", *Ain Shams Eng. J.,* **9(4)**, pp. 909–915 (2018).

24. Bhuvaneswari, M., Eswaramoorthi, S., Sivasankaran, S., et al. "Effect of viscous dissipation and convective heating on convection flow of a second grade fluid over a stretching surface: Analytical and numerical study", *Sci. Iran., B,* **26(3)**, pp. 1350–1357 (2019).

25. Gumber, P., Yaseen, M., Rawat, S.K., et al. "Heat transfer in micropolar hybrid nanofluid flow past a vertical plate in the presence of thermal radiation and suction/injection effects", *Partial Differential Equations in Applied Mathematics*, **5**, p. 100240 (2022).

26. Mallawi, O.M., Bhuvaneswari, M., Sivasankaran, S., et al. "Impact of double-stratification on convective flow of a non-Newtonian liquid in a Riga plate with Cattaneo-Christov double-flux and thermal radiation", *Ain Shams Eng. J.,* **12(1)**, pp. 969–981 (2021).

27. Noor, N.F.M., Ismoen, M., and Hashim, I. "Heat-transfer analysis of MHD flow due to a permeable shrinking sheet embedded in a porous medium with internal heat generation", *J. Porous Media*, **13(9)**, pp. 847–854.

28. Noor, N.F.M. and Hashim, I. "MHD viscous flow over a linearly stretching sheet embedded in a non-Darcian porous medium", *J. Porous Media*, **13(4)**, pp. 349–355 (2010).

29. Rana, S., Mehmood, R., and Bhatti, M.M. "Bioconvection oblique motion of magnetized Oldroyd-B fluid through an elastic surface with suction/injection", *Chin. J. Phys.*, **73**, pp. 314–330 (2021).

30. Kasmani, R.Md., Sivasankaran, S., Bhuvaneswari, M., et al. "Soret and Dufour effects on doubly diffusive convection of nanofluid over a wedge in the presence of thermal radiation and suction", *Sci. Iran., B,* **26(5)**, pp. 2817–2826 (2019).

31. Mallawi, O.M., Eswaramoorthi, S., Bhuvaneswari, M., et al. "Impact of double-diffusion and slip of order 2 on convection of chemically reacting Oldroyd-B liquid with Cattaneo-Christov dual flux", *Ther. Sci.,* **25**(5B), pp. 3729–3740 (2021).

32. Bejan, A. "A study of entropy generation in fundamental convective heat transfer", *ASME J. Heat Transf.,* **101**, pp. 718–725 (1979).

33. Bejan, A. "The thermodynamic design of heat and mass transfer processes and devices", *Heat Fluid Flow,* **8**, pp. 258–276 (1987).

34. Afridi, M.I. and Qasim, M. "Entropy generation in three dimensional flow of dissipative fluid", *Int. J. Appl. Comput. Math.,* **4**, pp. 1–11 (2018).

35. Alzahrani, A.K., Sivasankaran, S., and Bhuvaneswari, M. "Numerical simulation on convection and thermal radiation of Casson fluid in an enclosure with entropy generation", *Entropy,* **22**, p. 229 (2020).

36. Yildiz, C., Yildiz, A.E., Arici, M., et al. "Influence of dome shape on flow structure, natural convection and entropy generation in enclosures at different inclinations: A comparative study", *Int. J. Mech. Sci.,* **197**, p. 106321 (2021).

37. Shahsavar, A., Rashidi, M., Yildiz, C., et al. "Natural convection and entropy generation of Ag-water nanofluid in a finned horizontal annulus: A particular focus on the impact of fin numbers", *Int. Commun. Heat Mass Transf.*, **125**, p. 105349 (2021).

38. Shehzad, S.A., Hayat, T., Qasim, M., et al. "Effects of mass transfer on MHD flow of Casson fluid with chemical reaction and suction", *Braz. J. Chem. Eng.*, **30**(01), pp. 187–195 (2013).

39. Nadeem, S. and Hussain, S.T. "Analysis of MHD Williamson nano fluid flow over a heated surface", *J. Appl. Fluid Mech.,* **9**(2), pp. 729–739 (2016).

40. Bilal, S., Imtiaz Shah, M., Khan, N.Z., Akgul, A., et al. "Onset about non-isothermal flow of Williamson liquid over exponential surface by computing numerical simulation in perspective of Cattaneo Christov heat flux theory", *Alex. Eng. J.*, **61**(8), pp. 6139–6150 (2022).

41. Ijaz Khan, M., Alzahrani, F., Hobiny, A., et al. "Modeling of Cattaneo-Christov Double Diffusions (CCDD) in Williamson nanomaterial slip flow subject to porous medium", *J Mater. Res. Technol.,* **9(3)**, pp. 6172–6177 (2020).

42. Mahmood, A., Jamshed, W., and Aziz, A. "Entropy and heat transfer analysis using Cattaneo-Christov heat flux model for a boundary layer flow of Casson nanofluid", *Results Phys.,* **10**, pp. 640–649 (2018).

43. Bhatti, M.M., Abbas, T., and Rashidi, M.M. "Numerical study of entropy generation with nonlinear thermal radiation on magneto hydrodynamics non-Newtonian nanofluid through a porous shrinking Sheet", *J. Magn.*, **21**(3), pp. 468–475 (2016).

44. Eswaramoorthi, S., Bhuvaneswari, M., Sivasankaran, S., et al. "Soret and Dufour effects on viscoelastic boundary layer flow, heat and mass transfer in a stretching surface with convective boundary condition in the presence of radiation and chemical reaction", *Sci. Iran., B,* **23**(6), pp. 2575–2586 (2016).

Biographies

Sheniyappan Eswaramoorthi is an Assistant Professor in the Department of Mathematics at Dr. N. G.P. Arts and Science College, Coimbatore, Tamilnadu, India. He obtained his MSc and PhD degrees from Bharathiar University, Coimbatore, India. His areas of interest are boundary layer flow, and heat and mass transfer.

Sivanandam Sivasankaran received his MSc, MPhil, and PhD degrees from Bharathiar University, India. Then, he received Post-Doctoral Fellowship from National Cheng Kung University and National Taiwan University, Taiwan. He was a Research Professor at Yonsei University, South Korea. Also, he was an Assistant Professor at Sungkyunkwan University, South Korea, and Senior Lecturer at University of Malaya, Malaysia. Presently, he works at King Abdulaziz University, Saudi Arabia. He is an Associate Editor of three journals and a member of the editorial boards of several international journals. His areas of interest are convective heat and mass transfer, CFD, nanofluids, micro-channel heat sinks, and porous media.